# Thermal expansion and magnetovolume effects in the heavy-fermion system $Ce_2RhIn_8$

A. Malinowski, M. F. Hundley, N. O. Moreno, P. G. Pagliuso,* J. L. Sarrao, and J. D. Thompson
*Los Alamos National Laboratory, Los Alamos, New Mexico 87545, USA*
(Received 13 June 2003; published 20 November 2003)

We present the results of thermal expansion $\alpha(T)$, magnetostriction $\lambda(H,T)$, and specific-heat $C_p(T)$ measurements made on the heavy-fermion antiferromagnet $Ce_2RhIn_8$. The effects of magnetic order are clearly evident as anomalies in $\alpha(T)$ at $T_N=2.8$ K and at $T_m=1.65$ K. $C_p(T)$ data indicate that the upper transition corresponds to the onset of long-range antiferromagnetic order while the lower transition involves only a subtle rearrangement of the ordered state. Both $C_p/T$ and $\alpha/T$ grow with decreasing temperature below 20 K in a manner consistent with Kondo renormalization. Kondo interactions appear to be responsible for the large electronic Grüneisen parameter which extrapolates to $\Omega_e \approx 48$ as $T \rightarrow 0$, while the characteristic Kondo energy is $T_K \approx 10$ K as determined from the $C_p/T$ ratio at $T_N$. Above 20 K $\alpha(T)$ is dominated by crystalline-electric-field (CEF) effects. The data are consistent with a CEF level scheme consisting of excited $\Gamma_7^{(1)}$ and $\Gamma_6$ doublets lying $71\pm6$ K and $195\pm10$ K above a $\Gamma_7^{(2)}$ ground state. In the paramagnetic state ($T>T_N$) the volume magnetostriction follows a simple scaling law, $\lambda \propto [H/(T+T_\lambda)]^2$. The scaling parameter $T_\lambda=5$ K is consistent with the Kondo temperature determined from $\alpha(T)$ and $C_p(T)$ data. Analysis of $\lambda(H,T)$ data also indicates that the magnetic and electronic energy scales associated with the Kondo state in $Ce_2RhIn_8$ are equivalent. These thermodynamic data indicate that the physical properties of $Ce_2RhIn_8$ result from competition between magnetic exchange, Kondo, and CEF interactions.

DOI: 10.1103/PhysRevB.68.184419 PACS number(s): 75.80.+q, 71.27.+a, 65.40.De, 75.30.Kz

## I. INTRODUCTION

One of the most intriguing aspects of heavy-fermion (HF) compounds is the broad spectrum of possible ground states that they can exhibit. The ground state, by definition, characterizes a system in the zero-temperature limit and as such influences its behavior mainly in the low-temperature region. The excitations appearing at higher temperatures usually complicate the relatively simple situation in the low-$T$ region where one energy scale usually dominates. In HF systems, however, it is the high-T region which is better understood. This is partly because of a good separation of energy scales, at least in the $4f$ compounds. As in the case of conventional lanthanide compounds, a clear hierarchy of ionic energy is found, starting from the Coulomb interaction between the $f$ electrons on the order of 10 eV, direct exchange coupling, spin-orbit interaction, and down to crystal-field effects typically on the order of tens of meV (i.e., $\sim$100 K).[1] A clear separation of the electrostatic repulsion among the $f$-shell electrons and their spin-orbit coupling from the other energies leads to localized full-moment paramagnetism near room temperature. At low temperatures, however, the magnetic behavior is much more complicated due to competition between Kondo and the indirect exchange (Ruderman-Kittel-Kasuya-Yosida, RKKY) interactions. The energy scales that characterize these interactions are related to the exchange-coupling strength $J$ by $k_B T_K \sim E_F e^{-1/N(E_F)J}$ and $k_B T_N \sim E_F J^2$, respectively, where $T_K$ is the Kondo temperature, $T_N$ is the Néel temperature, $N(E_F)$ is the density of states at the Fermi energy $E_F$, and $k_B$ is the Boltzmann constant.[2] Of special interest are materials where these two energy scales are not well separated, i.e., where both the Néel temperature $T_N$ and the Kondo temperature $T_K$ are of the same order of magnitude. Some interesting deviations from the expected behavior described by Doniach's model[2] were recently found, for instance, in $Ce_3Pt_4In_{13}$.[3] Additional examples of materials where $T_N \sim T_K$ are $CeRhIn_5$ and $Ce_2RhIn_8$, the members of a new heavy-fermion family, $Ce_nM_mIn_{3n+2m}$, with $M=$ Co, Rh, Ir; $n=1$, 2; and $m=1$.

Because of its crystal structure and magnetic properties, $Ce_2RhIn_8$ may be regarded as a magnetic hybrid between $CeIn_3$ and $CeRhIn_5$.[4] $Ce_2RhIn_8$ is a HF antiferromagnet with $T_N=2.8$ K (Ref. 5) that becomes a superconductor under applied pressure of 1.63 GPa (the onset of zero resistivity occurs at $T_C=1.1$ K).[6] The high-temperature effective magnetic moment, taken from the susceptibility data above 200 K, shows a small anisotropy and is almost equal to the Hund's rule value for $J=5/2$ Ce ion, i.e., $2.54\mu_B$/Ce (namely, $2.53\mu_B$/Ce for magnetic field parallel to $ab$ plane and $2.47\mu_B$/Ce for magnetic field parallel to $c$ axis).[7] In the temperature interval 55–130 K the resistivity is proportional to $-\ln T$, consistent with single-impurity Kondo behavior. At around 4.5 K $\rho(T)$ exhibits a maximum, indicative of the onset of coherence.[8] The Sommerfeld constant for $Ce_2RhIn_8$, $\gamma \approx 400$ mJ/mole-CeK$^2$,[5] is close to the value of $\gamma$ for $CeRhIn_5$ just above $T_N$.[9] This $\gamma$ value qualifies $Ce_2RhIn_8$ as a HF compound, and it corresponds to a Kondo temperature[10] that is the same order of magnitude as $T_N$. As with $CeRhIn_5$, both $T_N$ and $\gamma$ decrease with the increasing applied magnetic field (along the tetragonal $c$ axis),[5] as one can expect for a HF.[11] While $\gamma$ for our $n=2$ member of the $Ce_nRhIn_{3n+2}$ family is similar to that of the $n=1$ compound, the ordered moment $\mu_0=0.55\mu_B$ (at $T=1.6$ K)[12] is very close to that for $CeIn_3$ ($0.48\mu_B$–$0.65\mu_B$),[13] which can be regard as $n=\infty$ member of this family. The magnetic moment of $Ce_2RhIn_8$ was found to point out from the $ab$ plane by 52°.[12] This ordered moment is smaller than for $CeRhIn_5$ (where $\mu_0=0.75\ \mu_B$)[14] suggesting that Kondo screening might be more effective in the less two dimensional $Ce_2RhIn_8$.

 

In this paper we present the results of temperature-dependent specific heat, anisotropic thermal expansion, and magnetostriction measurements on $Ce_2RhIn_8$ with the goal of clarifying the role of competing energy scales in determining this compound's macroscopic properties. The magnetic component of the $Ce_2RhIn_8$ thermal expansion, $\alpha_m(T)$, is strongly anisotropic at all temperatures and exhibits the influence of crystalline-electric-field(CEF) levels above 15 K. We use these data, in conjunction with anisotropic magnetic susceptibility data, to estimate a CEF level scheme for $Ce_2RhIn_8$. The scheme is composed of two magnetic doublets split from a doublet ground state by 70 and 195 K, respectively. Below 20 K $\alpha_m(T)$ is influenced both by Kondo renormalization and magnetic order. The electronic Grüneisen parameter rises sharply below 40 K, and approaches a value of roughly 20 before the material orders magnetically at $T_N$. Magnetostriction data in the paramagnetic state scale quadratically with applied field and the $T$ dependence is consistent with the Kondo energy scale determined from the enhanced Sommerfeld coefficient present in the specific heat $C_p(T)$ just above $T_N$. Thermal expansion, magnetostriction, specific heat, and resistivity data in the antiferromagnetic(AFM) state show evidence for an additional magnetic transition at 1.65 K that appears to be extremely sensitive to applied pressure. In total, the field- and temperature-dependent thermodynamic properties of $\alpha_m(T)$ are characteristic of a Kondo-compensated heavy-fermion antiferromagnet with comparable magnetic and Kondo energy scales.

## II. EXPERIMENT

$Ce_2RhIn_8$ samples used for thermal-expansion measurements were single crystals with dimensions $1\times1\times2$ mm$^3$ that were grown with a flux technique.[15] $Ce_2RhIn_8$ crystalizes in a quasi-two-dimensional tetragonal structure with lattice parameters at room temperature of $a=4.665$ Å and $c=12.244$ Å; no evidence for intergrowth of a $CeRhIn_5$ phase was found.[6] The same technique was also used to grow the non-$f$-electron counterpart $La_2RhIn_8$, with lattice parameters of $a=4.6780$ Å and $c=12.346$ Å.[16] The dimensions of the $La_2RhIn_8$ crystal used for thermal-expansion measurements were $2\times2\times2$ mm$^3$. With one formula unit per unit cell the molar volume of our compounds is $V_m=8.02\times10^{-5}$ m$^3$/mole-Ce in the case of Ce and $V_m=8.14\times10^{-5}$ m$^3$/mole-La in the case of La. Thermal-expansion measurements were performed in the temperature range from 1.4 to 300 K using an OFHC-copper capacitance dilatometer. The capacitance was measured using a 1-kHz Andeen-Hagerling 2500A capacitance bridge (resolution $10^{-7}$ pF). For our 2-mm specimen a detection limit of about 0.03 Å corresponds to a relative $\delta l/l$ resolution of roughly $\simeq10^{-9}$. The reported value of the linear thermal-expansion coefficient, $\alpha\equiv1/l(dl/dT)$, is corrected for cell effects, stemming from the thermal expansion of the copper cell.[17] Sample temperatures were determined with a Cernox temperature sensor.[18] To estimate the absolute accuracy of such obtained values of $\alpha$ we measured also a 4-mm-long cubic sample of pure aluminum. The deviations of experimental points from published data for aluminum[17] are typically $\sim\pm1\times10^{-7}$ K$^{-1}$ below 100 K. At higher temperatures the accuracy of $\alpha$ is lower because of small temperature gradients over the cell as well as thermal drifts present in our setup. Deviations from the published data above 150 K can be as high as $\sim\pm5\times10^{-7}$ K$^{-1}$ although typically they do not exceed $\pm3\times10^{-7}$ K$^{-1}$; this corresponds to roughly $\pm2\%$ of the measured $\alpha$. To observe magnetovolume effects a magnetic field of up to 3 T was applied parallel to the $ab$ plane and the relative change of the sample's length, both along the field direction and perpendicular to it, was measured. The typical field sweep rate for magnetostriction measurements was 26 mT/min and data points were taken with the field increasing and decreasing. Before each field sweep temperature was stabilized for 1–2 h and the capacitance signal was monitored to decrease the thermal drifts during the measurement. As a result the level of experimental uncertainty was reduced, typically below 1.5% of the total sample-length change between 0 and 3 T. We combined thermal expansion and magnetostriction results with magnetic-susceptibility data measured with a superconducting quantum interference device magnetometer and specific-heat data obtained with a Quantum-Design PPMS.

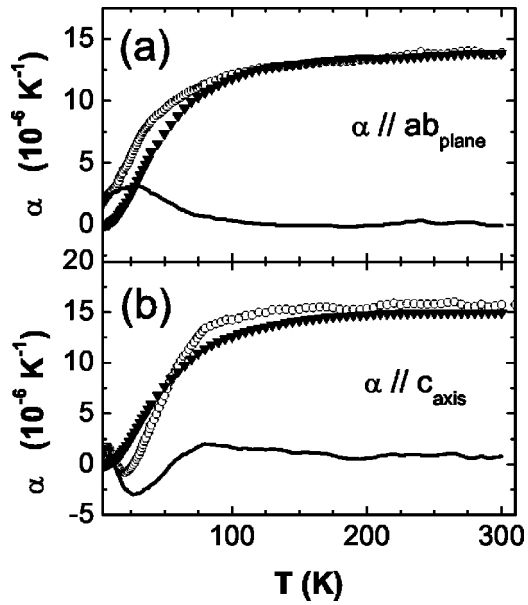


FIG. 1. The linear thermal expansion coefficients for $Ce_2RhIn_8$ (open circles) and $La_2RhIn_8$ (solid triangles) for temperatures $T$ above 4 K (a) in the $ab$ plane, and (b) along the $c$ axis. Solid lines correspond to the magnetic thermal expansion coefficients ($\alpha_m^{ab}$ and $\alpha_m^c$) obtained by subtracting the La data from the Ce data.

## III. RESULTS

In Fig. 1 we show the linear thermal-expansion coefficient of $Ce_2RhIn_8$ both in the $ab$ plane and along the $c$ axis, as a function of temperature for $T>4$ K. To estimate the lattice contribution to the $Ce_2RhIn_8$ thermal expansion we measured its nonmagnetic analog, $La_2RhIn_8$ (the conduction-electron contribution to the expansion coefficient of $La_2RhIn_8$ can be neglected). As can be seen in Fig. 1, $\alpha(T)$

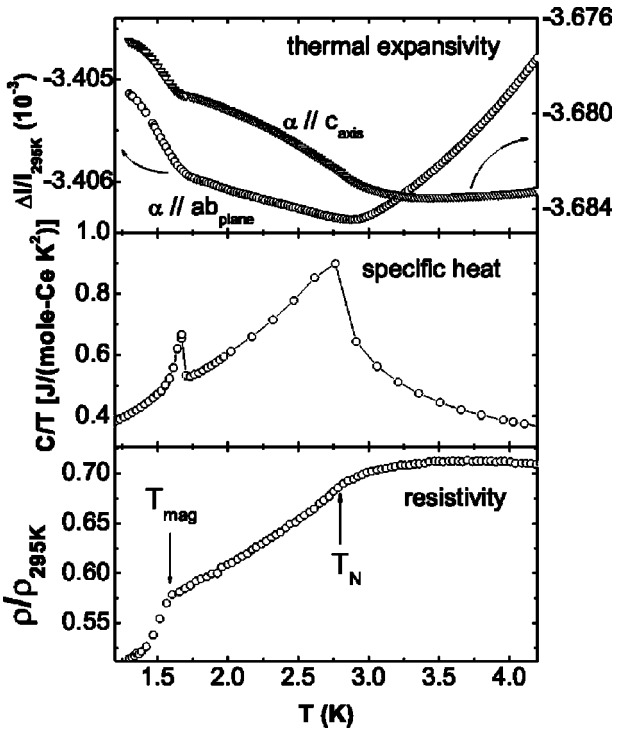


FIG. 2. The two magnetic transitions at $T_N = 2.8$ K and $T_m = 1.65$ K probed by three different techniques; from top to bottom: thermal expansivity, specific heat, and resistivity. The specific-heat measurements shown here were made on a small sample with dimensions $2 \times 1 \times 0.3$ mm$^3$, not sufficient for thermal-expansion measurements.

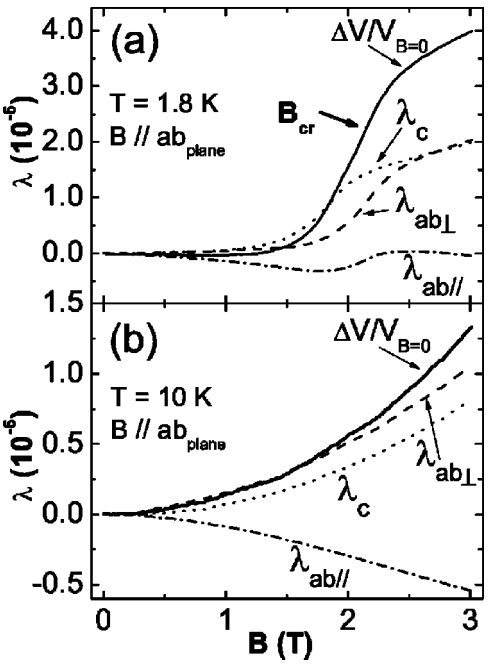


FIG. 3. Magnetostriction $\lambda = \Delta l / l_{B=0}$ for a magnetic field applied in the $ab$ plane at 1.8 K (a) and 10 K (b). Dotted lines depict the magnetostriction measured along the $c$ axis ($\lambda_c$), while dashed and dash-dotted lines correspond to in-plane magnetostriction measured perpendicular ($\lambda_{ab\perp}$) and parallel ($\lambda_{ab\parallel}$) to the applied field, respectively. The overall volume magnetostriction $\Delta V/V_0 = \lambda_c + \lambda_{ab\perp} + \lambda_{ab\parallel}$ is depicted by the solid line.

for $La_2RhIn_8$ displays temperature behavior typical for normal metals, decreasing smoothly with decreasing temperature. Only a small anisotropy exists between the $c$-axis ($\alpha_c$) and $ab$-plane ($\alpha_{ab}$) data—at room temperature $\alpha_c$ is larger than $\alpha_{ab}$ by only 8%. The volume thermal-expansion coefficient $\beta$ of $La_2RhIn_8$ calculated for tetragonal symmetry as $\beta = 2\alpha_{ab} + \alpha_c$, can be fitted well with the Debye model. The Debye temperature $\theta_D$ for which we obtain the best fit in the range 9–300 K is equal to 185 K and comparable with that obtained from fits to $La_2RhIn_8$ specific-heat data in the same temperature range (189 K). $\theta_D$ estimated from $a_1 T + a_2 T^3$ specific-heat fits at temperatures below 4 K is 147 K; the difference comes from well-known limitations of the Debye model.[19]

The thermal expansion for $Ce_2RhIn_8$ ($\alpha_{Ce}$) is much more anisotropic than is the case for $La_2RhIn_8$ ($\alpha_{La}$). In the $ab$ plane there is no detectable influence of $f$ electrons down to 120 K [see Fig. 1(a)], i.e., the values of $\alpha_{Ce}$ and $\alpha_{La}$ are almost equal. Below 120 K both $\alpha_{Ce}$ and $\alpha_{La}$ start to decrease much more rapidly with decreasing temperature than at higher temperatures, but $\alpha_{Ce}$ is larger than $\alpha_{La}$. This clearly indicates the appearance of an additional contribution to $\alpha_{Ce}$ beyond that due to the lattice. Along the $c$ axis [Fig. 1(b)] the temperature behavior of $\alpha_{Ce}$ is more complicated. At room temperature $\alpha_{Ce}$ is slightly higher than $\alpha_{La}$ and this situation persists down to roughly 55 K. At roughly 80 K $\alpha_{Ce}$ starts to decrease more rapidly than $\alpha_{La}$. Below 55 K $\alpha_{Ce}$ is smaller than $\alpha_{La}$. $\alpha_{Ce}$ exhibits a negative minimum near 20 K followed by an upturn towards positive values at lower temperatures. Two distinct features are present in the magnetic $Ce_2RhIn_8$ thermal-expansion contribution, $\alpha_{mag} = \alpha_{Ce} - \alpha_{La}$: along the $ab$ plane there is a positive peak with a maximum near 30 K, while along the $c$ axis there is an analogous negative peak centered at almost the same temperature (28 K). Both peaks can be attributed to crystal-field effects, as we will show later.

In the low-temperature region (see Fig. 2), in addition to the antiferromagnetic transition at $T_N = 2.8$ K,[20] $\alpha_{Ce}$ also shows evidence for a second magnetic transition at $T_m = 1.65$ K. This feature is clearly seen in three independent datasets made with quite different techniques: thermal expansivity, specific heat, and resistivity. The thermal expansivity data depicted in Fig. 2 show that in the paramagnetic regime ($T > 2.8$ K) $Ce_2RhIn_8$ shrinks with decreasing temperature both along the $c$ axis and within the $ab$ plane. At the Néel temperature $Ce_2RhIn_8$ stops shrinking and it expands very slowly in the $ab$ plane and at a faster rate along the $c$ axis. At $T_m = 1.65$ K $Ce_2RhIn_8$ begins to expand even faster in both directions. Both magnetic transitions at $T_N$ and $T_m$ are clearly seen as cusps in the specific-heat data. Curiously, while $T_N$ is marked only as a subtle change in the slope of $\rho(T)$, the change at $T_m$ is far more dramatic.

To see how a magnetic field changes the transition temperature $T_m$ we measured the magnetostriction in several fields to 3 T, applied in the $ab$ plane. Because of the tetragonal symmetry of $Ce_2RhIn_8$ the volume magnetostriction, $\lambda_V \equiv \Delta V/V_0$, is determined by measuring the linear magne-

tostriction, $\lambda \equiv \Delta l/l_0$, along the $ab$ plane both parallel to the applied field, $\lambda_{ab\|}$, and perpendicular to it, $\lambda_{ab\perp}$. The representative magnetostriction curves at 1.8 K are shown in Fig. 3(a). Along the applied field direction ($\Delta l \| B$) the sample contracts but the final volume magnetostriction, calculated as $\lambda_V = \lambda_{ab\|} + \lambda_{ab\perp} + \lambda_c$, is positive, because the sample expands perpendicularly to the field. The critical field $B_{cr}$ defined as the maximum in the derivative $d\lambda_V/dB$ increases with increasing temperature above 1.6 K. Its values $B_{cr}(T)$ agree well with those obtained from magnetoresitivity measurements.[8]

In the paramagnetic region ($T > T_N$) an applied field in the $ab$ plane also acts to contract the sample in the direction of the field ($\lambda_{ab\|}$ is negative) while expanding it in the perpendicular directions, both in the $ab$ plane and along the $c$ axis ($\lambda_{ab\perp}$ and $\lambda_c$ are positive)—the data are shown in Fig. 3(b). This suggests that the direction of the field is more important than crystal symmetry in determining the magnetostriction. The paramagnetic magnetostriction was measured at 3, 3.5, 5, 10, 15, and 20 K. The volume magnetostriction is positive and proportional to $B^2$, as one can expect for a paramagnet.[21] The amplitude of the volume magnetostriction increases with increasing temperature up to 5 K, while above 5 K it starts to decrease.

## IV. DISCUSSION

In the following section we will describe the rich thermodynamics of $Ce_2RhIn_8$ by separating the different effects coming from Kondo, RKKY, and CEF interactions. First we concentrate on the magnetic transition found at $T_m = 1.65$ K, show how it is influenced by magnetic field, and predict the pressure dependence of both $T_m$ and $T_N$. Next, in Sec. IV B, we examine the strong competition between magnetic and Kondo interactions in the ordered state, below $T_N$, clearly seen in the specific-heat data. In Sec. IV C we focus on still higher temperatures where CEF effects dominate. A careful analysis of the thermal-expansion data allows us to estimate the CEF levels splittings. Section IV D is devoted to the Grüneisen analysis of $\alpha(T)$ and $C_p$. Calculating the electronic Grüneisen parameter allows an estimate of the volume dependence of the characteristic temperatures found in the previous subsections and confirms the Kondo-driven mass renormalization at low temperatures in $Ce_2RhIn_8$. Finally, in Sec. IV E, we expand the Grüneisen analysis to include a magnetic-field scaling parameter. We calculate the magnetic Grüneisen parameter from the magnetostriction data in the paramagnetic state to check whether the magnetic and thermal energy scales are equivalent in $Ce_2RhIn_8$. We also show that the magnetostriction in the paramagnetic state follows a simple scaling law, originating from general thermodynamics.

### A. Two magnetic transitions and the magnetic phase diagram

Before focusing on the competition between Kondo and RKKY-mediated magnetic interactions in $Ce_2RhIn_8$, we will first examine the magnetic phase diagram. Below 5 K two magnetic transitions are clearly evident in the thermal expansion, specific-heat, and resistivity data presented in Fig. 2. The data in Fig. 2 indicate that the sample length varies continuously across both transitions. The entropy, obtained by integrating $C_p/T$ versus temperature, also appears to be continuous across both transitions. The variation of the volume thermal expansion $\beta(T)$ in the vicinity of the two magnetic transitions is shown in Fig. 4. The steplike feature at $T_N$ in $\beta(T)$ and the mean-field-like anomaly in $C_p(T)$ at the same temperature are consistent with a second-order magnetic-phase transition. The thermodynamic nature of the transition at $T_m$ is less clear. The sharp feature in $\beta(T)$ near $T_m$ suggests that this is a first-order transition whereas the absence of any latent heat in the specific-heat data suggests instead that this is a second-order transition. This inconsistency could stem from the fact that the lower transition is extremely pressure dependent. Recent pressure-dependent measurements of $T_m$ give a pressure derivative $dT_m/dp = -4.3 \pm 1.5$ K/kbar, a value that is roughly 60 times bigger than the pressure dependence of the transition at $T_N$ ($dT_N/dp = -76$ mK/kbar).[6] The very large pressure dependence of the lower transition temperature means that this transition will be very sensitive to any external or internal strain. The specific-heat signature of the lower transition is extremely sample dependent, with some samples exhibiting a weak (or undetectable) anomaly at 1.65 K.[5] In comparison, the specific-heat signature associated with the transition at $T_N$ shows no sample-to-sample variation. These facts suggest that the phase transition at $T_m$ could be a first-order transition that is broadened by internal strain. Recent preliminary diffraction measurements confirm that strain is present in $Ce_2RhIn_8$.[22]

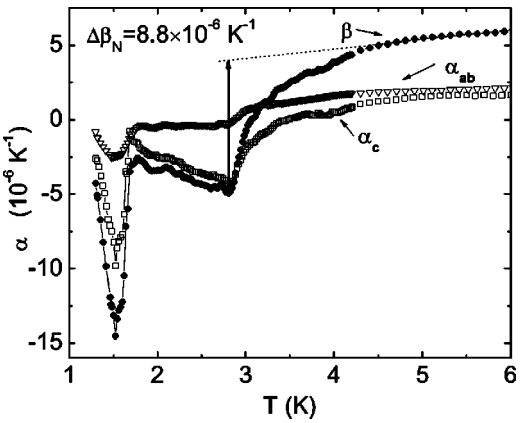


FIG. 4. The linear (open symbols) and volume expansion (solid symbols) coefficients for $Ce_2RhIn_8$ in the vicinity of the magnetic transitions. The dashed line indicates the interpolation used to calculate the jump in $\beta$ at $T_N$ and $T_m$.

In determining the thermodynamic nature of a phase transition it is useful to compare predicted and experimental values of the transition-temperature pressure derivatives. The Clausius-Clapeyron equation and the Ehrenfest relationship equate $dT_c/dp$ to the changes in thermodynamic variables that occur at a first- and second-order transition, respectively. The Clausius-Clapeyron equation relates $dT_c/dp$ to the volume change $\Delta V$ and entropy change $\Delta S$ that occur at a first-order transition:

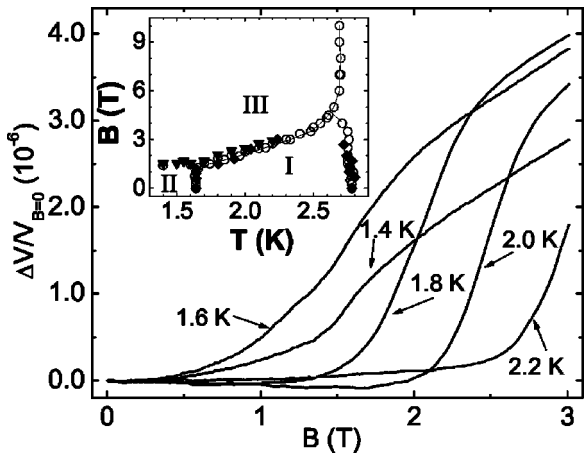


FIG. 5. The magnetovolume effect as a function of field in the magnetically ordered state for $Ce_2RhIn_8$. The magnetic phase diagram is shown in the inset. The phase diagram is composed from magnetoresistance data[8] (open circles), constant-$B$ thermal-expansion data (solid diamonds), and constant-$T$ magnetovolume measurements (solid triangles).

$$\frac{dT_c}{dp} = \frac{\Delta V}{\Delta S}. \tag{1}$$

The Ehrenfest relationship relates $dT_c/dp$ to the changes in the volume thermal expansion, $\Delta\beta$, and heat capacity, $\Delta C_p$, that occur at a second-order transition:

$$\frac{dT_c}{dp} = V_m T_c \frac{\Delta\beta}{\Delta C_p}, \tag{2}$$

where $V_m$ is the molar volume. To calculate the pressure derivatives of both transition temperatures, $T_N$ and $T_m$, we use values of $\Delta C_p$ and $\Delta S$ measured on the same sample that was used in making our thermal-expansion measurements. For the upper (second-order) transition $\Delta C_p(T_N) = -2.7 \pm 0.4$ J/mole-Ce K. The dashed line in Fig. 4 indicates the interpolation used to calculate the jump in $\beta$ at $T_N$. The Ehrenfest estimate for the upper transition $dT_N/dp = -73 \pm 17$ mK/kbar is in good agreement with that found in the hydrostatic pressure measurements where the initial slope $dT_N/dp$ was estimated to be $-76$ mK/kbar.[6] For the lower transition an estimate for $\Delta V$ and $\Delta S$ can be obtained by integrating the anomalies centered at 1.65 K in $\beta$ and $C_p/T$, respectively; the experimental values for these quantities ($\Delta V = -2.2 \pm 0.4 \times 10^{-10}$ m$^3$/mole-Ce and $\Delta S = 4.2 \pm 0.7$ mJ/mole-Ce K) can be combined with the Clausius-Clapeyron equation to estimate the pressure derivative of $T_m$. The pressure derivative so determined ($dT_m/dp = -5.2 \pm 1.3$ K/kbar) is in reasonable agreement with the experimental value of $dT_m/dp = -4.3 \pm 1.5$ K/kbar.[6] Given the large uncertainty in these $dT_m/dp$ values, it would be wrong to conclude that the similarity in the measured and calculated pressure-derivative values proves that the transition at $T_m$ is first order. At most, we can say that the thermal-expansion, specific-heat, and pressure-dependent transition temperature measurements are consistent with the presence of a strained first-order magnetic transition at $T_m$.

To clarify the influence of an applied magnetic field on the lower transition temperature $T_m$, thermal expansion at constant $B$ and magnetostriction at constant $T$ were measured. The linear magnetostriction along all three directions ($\lambda_c$, $\lambda_{ab\parallel}$, and $\lambda_{ab\perp}$) displays large slope changes at the fields above 1 T, as is shown for example for $T = 1.8$ K in Fig. 3(a). As shown in Fig. 5, the volume magnetostriction is positive in the magnetically ordered state. The critical field value $B_{cr}$ taken as the points where $\partial\lambda_V/\partial B$ is a maximum, together with the values of critical temperature $T_{cr}$, where the sharp feature in the $\alpha(T)$ curves occurs, can be combined to construct a magnetic phase diagram for $B \leqslant 3$ T; this phase diagram is shown in the inset of Fig. 5. These points collapse very well on the phase diagram boundaries obtained from magnetoresitivity measurements.[8] $B_{cr}$ is essentially $T$ independent below 1.7 K, while it rises with increasing temperature above this point. The critical temperature does not depend on the field up to 1.5 T and it starts to increase with increasing field above 1.5 T. Preliminary magnetotransport[8] and neutron-diffraction measurements[23] suggest that magnetic phases II and III (see the inset in Fig. 5) are only slightly altered from the antiferromagnetic incommensurate[23] phase I, with the transition from phase I to II involving the development of a commensurate component.

### B. RKKY and Kondo interactions

Strong competition between magnetic exchange and Kondo interactions will occur in any compound in which the magnetic ordering temperature $T_N$ is comparable to the Kondo energy scale $T_K$. The electronic contribution to the specific-heat of $Ce_2RhIn_8$ just above $T_N$ approaches $\gamma = 400$ mJ/mole-Ce K$^2$.[9] The Sommerfeld coefficient is still quite large in the magnetic ground state (the zero-temperature limit of the electronic specific-heat coefficient is $\gamma_0 = 370$ mJ/mole-Ce K$^2$).[5] These large $\gamma$ values categorize $Ce_2RhIn_8$ as a heavy-fermion compound. Within the framework of the Coqblin-Schrieffer model[24] the large renormalized $\gamma$ in the paramagnetic state just above $T_N$ corresponds to a Kondo scale $T_K \approx 10$ K.[10] Further evidence for a Kondo-compensated magnetic state is provided by the reduced ordered moment ($\mu_0 \approx 0.55\mu_B$) evident below $T_N$ and the limited magnetic entropy liberated at the ordering temperature ($S \approx 30\%$ of $R \ln 2$ at $T_N$). The full $R \ln 2$ entropy associated with the doublet ground state is only achieved when the specific-heat data are integrated up to roughly 20 K, indicating that the low-temperature thermodynamics of $Ce_2RhIn_8$ is characteristic of overlapping Kondo and RKKY interactions.

The Kondo-compensated magnetic states in the sister compounds $Ce_2RhIn_8$ and $CeRhIn_5$ are quite similar but also display some important differences. Both compounds order magnetically with Neel temperatures of 2.8 and 3.8 K, respectively, and they both have low-temperature paramagnetic-state Sommerfeld coefficient of roughly 400 mJ/mole-Ce K$^2$.[9] The ordered magnetic moment for both compounds is roughly $(0.65 \pm 0.1)\mu_B$.[12,14] Magnetic entropy calculations based on specific-heat data indicate that only 30% of the doublet ground-state entropy is liberated at $T_N$ in both compounds; the remaining ground-state entropy resides

in the Kondo-induced rise in $C/T$ that occurs in both compounds below 20 K. Both compounds also share a similar CEF level scheme (see below). Differences between the compounds only become apparent below their respective ordering temperatures. While most of the enhanced paramagnetic Sommerfeld coefficient is still present below $T_N$ in $Ce_2RhIn_8$, 85% of the large paramagnetic $\gamma$ in $CeRhIn_5$ is eliminated in the ordered state ($\gamma_0 = 56$ mJ/mole-Ce $K^2$) due to the formation of a spin-density wave that gaps most of the Fermi surface.[5] In addition, the $T^3$ magnon contribution to the $T < T_N$ specific-heat in $Ce_2RhIn_8$ is roughly five times larger than that of $CeRhIn_5$. The similarities in the ordered moments, the paramagnetic Sommerfeld coefficients, the magnetic entropy liberated at $T_N$, and the RKKY and Kondo energy scales indicate that the thermodynamics of the Kondo-compensated ground states are quite similar in both compounds, while any differences reside in the details surrounding their respective magnetically ordered ground states. The drastic difference in the residual resistivity $\rho_0$ values ($\rho_0$ of $Ce_2RhIn_8$ is over 100 times larger than that of $CeRhIn_5$) was recently suggested to be caused by the difference in the crystallographic structure (namely, the buckling of the $Rh\text{-}In_3$ layer in $Ce_2RhIn_8$) rather than by the magnetic effects.[16] Similar differences in $\rho_0$ are also observed in nonmagnetic analogs where the buckling of Rh atom is even bigger.[16]

### C. Crystal-field effects

Above roughly 20 K the thermodynamic properties of $Ce_2RhIn_8$ are no longer dictated by magnetic order or Kondo renormalization, but are instead dominated by crystal-field effects. Clear evidence for this is found in the magnetic thermal expansion data shown in Fig. 1. The broad peaks centered at roughly 30 K in both $\alpha_m^{ab}$ and $\alpha_m^c$ are characteristic of CEF effects observed in many *f*-electron systems.[25] $Ce_2RhIn_8$'s CEF scheme can be determined by analyzing these anisotropic thermal-expansion coefficients within the context of a point-charge model.[26] In the presence of tetragonal crystal symmetry the $Ce^{3+}$ $J = 5/2$ multiplet splits into three doublets with angular-momentum wave functions that are a mixture of spin states $|1/2\rangle$, $|3/2\rangle$, and $|5/2\rangle$:[27]

$$\Gamma_7^{(1)} = \eta|\pm 5/2\rangle + \sqrt{(1-\eta^2)}|\mp 3/2\rangle,$$

$$\Gamma_7^{(2)} = \sqrt{(1-\eta^2)}|\pm 5/2\rangle - \eta|\mp 3/2\rangle,$$

$$\Gamma_6 = |\pm 1/2\rangle, \tag{3}$$

where $\eta$ is a mixing constant that can range between 0 and 1. Following the work of Morin *et al.*[28] and Lacerda *et al.*[25] the thermal-expansion coefficients for a system with tetragonal symmetry are

$$\alpha_m^c = (C_1 + \sqrt{2}C_2) f_{CEF}(T), \tag{4a}$$

$$\alpha_m^{ab} = \left( C_1 - \frac{1}{\sqrt{2}} C_2 \right) f_{CEF}(T), \tag{4b}$$

where the coefficients $C_1$ and $C_2$ are *T*-independent parameters related to elastic constants and magnetoelastic coupling parameters. The function $f_{CEF}(T)$ in Eqs. (4) is the temperature derivative of the Stevens quadrupolar operator expectation value $f_{CEF}(T) = d\langle O_2^0 \rangle / dT$. With the eigenstates appropriate for tetragonal symmetry [listed in Eqs. (3)], the temperature-dependent Stevens quadrupolar operator expectation value is given by

$$\langle O_2^0 \rangle (T) = \frac{10 + 2(6\eta^2 - 1)e^{-\Delta_1/k_BT} - 8e^{-\Delta_2/k_BT} - 12\eta^2}{1 + e^{-\Delta_1/k_BT} + e^{-\Delta_2/k_BT}}, \tag{5}$$

where $k_B$ is the Boltzmann constant, $\Delta_1$ is the energy splitting between the $\Gamma_7^{(1)}$ and $\Gamma_7^{(2)}$ states, and $\Delta_2$ is the energy splitting between the $\Gamma^6$ and $\Gamma_7^{(2)}$ states. For the point-charge model the temperature dependence of the thermal-expansion coefficients is wholly contained within the function $f_{CEF}(T)$. As such the model predicts that $\alpha_m^{ab}$ and $\alpha_m^c$ should only differ in the multiplicative constants that appear in front of $f_{CEF}(T)$. In comparing this prediction to the data shown in Fig. 1, it appears that $\alpha_m^{ab}$ and $\alpha_m^c$ both exhibit much the same temperature dependence while differing only in having prefactors that are of opposite sign. Both quantities exhibit a broad peak centered near 30 K and gradually tail off towards zero above 100 K. The presence of a modest peak in $\alpha_m^c$ at roughly 75 K that is not evident in $\alpha_m^{ab}$ indicates that the point-charge prediction is not entirely borne out. The fact that there is some difference between the data and the qualitative predictions of the point-charge model is not surprising given the presence of itinerate electrons and Kondo interactions in $Ce_2RhIn_8$. Nonetheless, the point-charge model does appear to capture the general features present in the temperature-dependent magnetic thermal-expansion coefficients in both directions.

Determining the CEF level scheme from magnetic thermal-expansion coefficients amounts to fitting temperature-dependent thermal-expansion data to the function $f_{CEF}(T)$ in order to estimate the parameters $\Delta_1$, $\Delta_2$, and $\eta$. In fitting the magnetic thermal-expansion data, it is advantageous to fit a physical quantity that combines both $\alpha_m^{ab}$ and $\alpha_m^c$. For weakly anisotropic materials the volume magnetic thermal-expansion coefficient $\beta_m = 2\alpha_m^{ab} + \alpha_m^c$ is the quantity of choice. For $Ce_2RhIn_8$ $\alpha_m^{ab}$ and $\alpha_m^c$ are nearly equal but of opposite sign, so that the experimental quantity $\beta_m$ is small, dominated by $\alpha_m^{ab}$ and suffers from large experimental error. As such, a more accurate CEF level scheme can be determined by fitting the anisotropic thermal-expansion parameter defined as $\alpha_{aniso} \equiv \alpha_m^c - (1/3)\beta_m = (2/3)(\alpha_m^c - \alpha_m^{ab})$. $\alpha_{aniso}$ is defined in such a way that it will be zero for an isotropic system (i.e., for $\alpha_m^c = \alpha_m^{ab}$ $\alpha_{aniso} = 0$). In terms of the thermal function $f_{CEF}(T)$ and the constants defined in Eqs. (4) the anisotropic thermal-expansion parameter is

$$\alpha_{aniso}(T) = \sqrt{2}C_2 f_{CEF}(T). \tag{6}$$

The anisotropy inherent in the wave functions that make up the CEF levels give rise to the strong anisotropy evident in

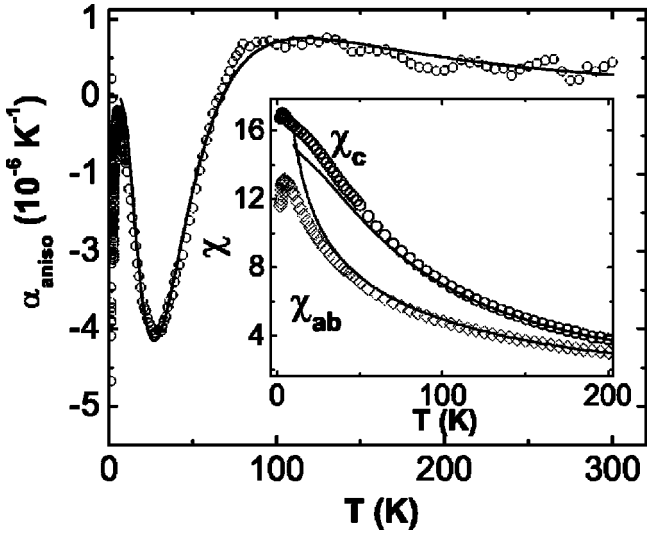


FIG. 6. The anisotropic thermal expansion coefficient $\alpha_{aniso}$ plotted as a function of temperature. Measured values are denoted by open circles while the solid lines show the calculated $\alpha_{aniso}$ based on Eqs. (5) and (6) with $\Delta_1 = 71$ K, $\Delta_2 = 195$ K, and $\eta = 0.85$. The inset compares the measured $ab$ plane (diamonds) and $c$ axis (circles) magnetic susceptibility with the fits (solid lines) to Eq. (7) with an isotropic molecular-field constant $\lambda = -30$ mole/emu and the CEF parameters listed above. The units for the susceptibility axis are $10^{-3}$ emu/mole-Ce.

the magnetic thermal-expansion coefficients. Hence $\alpha_{aniso}(T)$ data contain more information about the CEF levels than do $\beta_m(T)$ data, so fitting the anisotropic parameter produces a more reliable CEF level scheme.

To obtain the most accurate CEF level scheme we *simultaneously* fit $\alpha_{aniso}(T)$ and the in-plane and out-of-plane magnetic susceptibility $\chi_{ab}(T)$ and $\chi_c(T)$. The susceptibility is fit to the formula

$$\chi^{-1} = \chi_{CEF}^{-1} - \lambda, \tag{7}$$

where $\chi_{CEF}$ is the susceptibility of the CEF levels in tetragonal symmetry,[27] and $\lambda$ is a phenomenological molecular-field constant that is included to account for magnetic exchange effects. The level scheme that provides the best fit to $\alpha_{aniso}(T)$ and $\chi(T)$ simultaneously in the temperature range from 15 to 300 K consists of a $|3/2\rangle$-rich $\Gamma_7^{(2)}$ ground state, a $|5/2\rangle$-rich $\Gamma_7^{(1)}$ first excited state, and a highest-lying $\Gamma_6$ state. The energy splittings of the levels are $\Delta_1 = 71 \pm 6$ K and $\Delta_2 = 195 \pm 10$ K (note that $\Delta_2$ corresponds to the energy splitting between the ground-state doublet and the $\Gamma_6$ level). The mixing parameter and molecular-exchange constant are $\eta = 0.85 \pm 0.02$ and $\lambda = -30 \pm 3$ mole/emu, respectively. This level scheme is very similar to the scheme determined for $CeRhIn_5$ by inelastic neutron-scattering measurements.[29] The fits to the $Ce_2RhIn_8$ $\alpha_{aniso}$, $\chi_{ab}$, and $\chi_c$ data utilizing these parameters are depicted in Fig. 6. The CEF parameters provide an excellent fit to the experimental $\alpha(T)$ data; in particular, the negative peak at 30 K and the broad maximum at 100 K are both fit quite well. The agreement between the experimental susceptibility data and the fits are also good above 50 K. The molecular-field constant contributes to the inverse of $\chi$ as $(T_K + T_N)/C_{J=5/2}$ at high temperatures. With $T_N = 2.8$ K and $C_{J=5/2} = 0.80$ emu/(K mole), the $\lambda$ value obtained from the fit corresponds to a "high-temperature" Kondo temperature $T_K \approx 21$ K. This is very similar to the "low-$T$" Kondo temperature established from $C/T$ data near $T_N$. The $\chi$ fits deviate from the data below 50 K in both directions in a manner similar to that of $CeRhIn_5$ when CEF parameters found from the neutron-scattering measurements are used to fit susceptibility data.[29,30] This deviation stems from the fact that the fitting model utilized to produce the susceptibility fits [Eq. (7)] does not fully account for the influence of Kondo interactions on the CEF-derived anisotropic magnetic susceptibility. The fits to the $Ce_2RhIn_8$ susceptibility can be improved, particularly below 50 K, by employing anisotropic exchange parameters, but it is unclear if the resulting $\lambda_{ab}$ and $\lambda_c$ parameters are anything more than curve-fitting parameters that mimic a more sophisticated microscopic description of the CEF susceptibility in the presence of Kondo interactions. Although this approach can improve the $\chi(T)$ fits, it does not change the CEF level scheme or the energy splitting therein.[31]

When comparing the CEF level schemes for $CeIn_3$,[32] $CeRhIn_5$,[29] and $Ce_2RhIn_8$, a smooth evolution from $n = \infty$ to $n = 1$ member of the $Ce_nRhIn_{3n+2}$ family can be clearly seen. The ground-state wave function in each compound is a mixture of $|5/2\rangle$ and $|3/2\rangle$ states. The fourfold degenerate $\Gamma_8$ state in cubic $CeIn_3$ (135 K above the ground-state level)[32] is split into two doublets, $\Gamma_7^{(2)}$ and $\Gamma_6$, in the tetragonal symmetry of the surrounding ions in $Ce_2RhIn_8$ and $CeRhIn_5$. While $\Delta_1$ is practically the same in both these compounds, the energy splitting between the ground state and the second energetic level, $\Delta_2$, increases by about 40% when going from $Ce_2RhIn_8$ to the more two dimensional $CeRhIn_5$. A similar trend was observed in the isostrucutural antiferromagnetic non-Kondo systems $Nd_nMIn_{3n+2}$ ($M$ = Rh, Ir; $n = 1, 2$).[33]

### D. Electronic Grüneisen parameter

By combining thermal-expansion and specific-heat data to calculate the electronic Grüneisen parameter, it is possible to more clearly determine the thermodynamic character of the various interaction mechanisms present in $Ce_2RhIn_8$. The total Grüneisen parameter, $\Omega_T$, defined by

$$\Omega_T = V_m B_T \frac{\beta}{C_V}, \tag{8}$$

links the volume thermal-expansion coefficient $\beta$ and the constant-volume specific heat $C_V$. In Eq. (8) $V_m$ is the molar volume and $B_T$ is the isothermal bulk modulus. The Grüneisen parameter defined in Eq. (8) encompasses all thermodynamic contributions to $\beta$ and $C_V$. In an $f$-electron system these contributions will come from conventional phonon excitations, Kondo interactions, crystal-field excitations, and magnetic-exchange (RKKY) interactions. If each such interaction makes a contribution $C_i$ to the total specific heat $C_T$

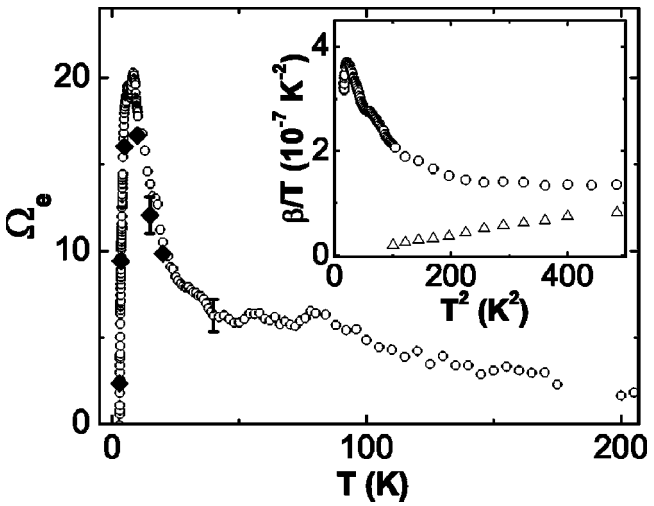


FIG. 7. The electronic $\Omega_e$ (open circles) and magnetic $\Omega_H$ (solid diamonds) Grüneisen parameters plotted as a function of temperature for $Ce_2RhIn_8$. The error bar at 40 K depicts the representative estimated error for $\Omega_e$. The error bar at $T=15$ K shows error connected with $\Omega_H$. (Ref. 43) In the inset the total volume thermal expansion is plotted as $\beta/T$ vs $T^2$ for both $Ce_2RhIn_8$ (circles) and $La_2RhIn_8$ (triangles).

$=\Sigma_i C_i$, the Grüneisen parameters stemming from each interaction $\Omega_i$ are related to the total Grüneisen parameter by[34]

$$\Omega_T=\frac{1}{C_T}\sum_i \Omega_i C_i. \tag{9}$$

The power of Grüneisen analysis lies with the fact that the Grüneisen parameter related to a particular interaction is a measure of that interaction's volume dependence. This is clear from the definition of the Grüneisen parameter,

$$\Omega_i=-\frac{V}{U_i}\frac{\partial U_i}{\partial V}, \tag{10}$$

where $U_i$ is an energy scale parameter that characterizes the interaction in question, and $V$ is the system volume. Examples of various interaction mechanisms and their associated energy scale parameter include (1) lattice excitations where the relevant scale parameter would be a phonon frequency $\omega_0$; (2) conventional electronic excitations at the Fermi energy, $E_F$, where the relevant scale parameter is the Fermi-energy density of states $N(E_F)$; (3) the Kondo interaction with the Kondo temperature $T_K$ acting as the scale parameter; (4) crystal-field excitations with the level-splitting energy acting as the scale parameter; and (5) magnetic interactions with the magnetic ordering temperature acting as the scale parameter. The Grüneisen parameter in a nonmagnetic system is quite small ($\Omega\approx 1$ to 2) because phonon frequencies and the Fermi-energy density of states are weakly volume dependent; the free-electron Grüneisen parameter, as determined from the volume derivative of the $N(E_F)$, is $\Omega=2/3$. In comparison, heavy-fermion systems have a very large Grüneisen parameter because the underlying Kondo interaction is strongly volume-dependent. A simple estimate of the Grüneisen parameter of a Kondo system can be made by combining an expression for the Kondo temperature with one that enumerates the relationship between the magnetic exchange constant and unit-cell volume. For a spin-1/2 Kondo impurity in a metallic host, $T_K=(E_F/k_B)\exp[-1/|J|N(E_F)]$, where $J$ is the magnetic exchange constant; the magnetic exchange constant is related to the unit-cell volume by $|J|=|J_0|V^{-n}$. The resulting Grüneisen parameter is $\Omega=n\ln(k_BT_K/E_F)$. With a 10 K Kondo temperature, a 1 eV Fermi energy, and $n=6$,[35] the estimated Grüneisen parameter will be $\Omega=42$, a value much larger than that of a free-electron system.

The many-body Kondo interactions that produce the enhanced electronic specific-heat contribution below 20 K in $Ce_2RhIn_8$ also enhance significantly the thermal-expansion coefficient in the same temperature range. The low-temperature volume thermal-expansion coefficient is expected to follow the same Debye-model temperature dependence as the specific heat,

$$\beta=a_1T+a_2T^3, \tag{11}$$

where $a_1$ and $a_2$ are the constants that characterize electronic and lattice contributions, respectively.[36] The volume thermal-expansion coefficients of both $Ce_2RhIn_8$ and $La_2RhIn_8$ are plotted as $\beta/T$ versus $T^2$ in the inset to Fig. 7. The $La_2RhIn_8$ data exhibit the expected Debyelike linear behavior with a constant slope and a very small intercept. In comparison, the $Ce_2RhIn_8$ data differ markedly from the expected Debye behavior; $\beta/T$ rises rapidly below 15 K, and reaches a maximum value just above the point where magnetic order produces a sharp drop in the data. The $La_2RhIn_8$ data indicate that the lattice contribution is small and entirely conventional, so that the rise in the $Ce_2RhIn_8$ data must be associated with the electronic thermal-expansion coefficient $a_1$. The maximum value of $\beta/T$ corresponds to a linear coefficient $a_1\approx 4\times10^{-7}$ $K^{-2}$. This value is comparable to that of the moderately heavy compounds $CeBe_{13}$ ($a_1=2.7\times10^{-7}$ $K^{-2}$, $\gamma=155$ mJ/mole $K^2$)[37] and $UAl_2$ ($a_1=1.0\times10^{-6}$ $K^{-2}$, $\gamma=133$ mJ/mole $K^2$),[38] but it is small compared to heavily mass-renormalized systems such as $CeAl_3$ ($a_1=-1.3\times10^{-4}$ $K^{-2}$, $\gamma=1.5$ J/mole $K^2$)[39] and $CeCu_2Si_2$ ($a_1=9\times10^{-6}$ $K^{-2}$, $\gamma=1.0$ J/mole $K^2$).[40] $Ce_2RhIn_8$'s enhanced electronic thermal-expansion coefficient is consistent with the enhanced Sommerfeld coefficient ($\gamma\approx 400$ mJ/mole $K^2$), evident in $C/T$ data above $T_N$. The enhancement of both parameters is a clear indication that the carrier mass in $Ce_2RhIn_8$ is Kondo renormalized below 20 K.

The renormalized heavy-fermion state usually exhibits an anomalously large electronic Grüneisen parameter as well. The electronic Grüneisen parameter $\Omega_e$ can be determined from the magnetic contributions to the specific heat $C_m$ and volume thermal expansion $\beta_m$.[41] The magnetic contributions to $\beta$ and $C_p$ are determined by subtracting $La_2RhIn_8$ thermal expansion or specific-heat data from the appropriate $Ce_2RhIn_8$ data. The electronic Grüneisen parameter is related to magnetic contributions to the thermal expansion and specific-heat by

$$\Omega_e = V_m B_T \frac{\beta_m}{C_m}, \tag{12}$$

where $\Omega_e$ encompasses all thermodynamic interactions (CEF, Kondo, and magnetic exchange) that are not present in the nonmagnetic $La_2RhIn_8$ compound. The temperature-dependent electronic Grüneisen parameter for $Ce_2RhIn_8$ is plotted in Fig. 7; for purposes of determining $\Omega_{el}$, the bulk modulus of $CeRhIn_5$ ($B_T = 780$ kbar) was used in the calculations.[42] $\Omega_e$ at 200 K is roughly 2, a value that is only slightly higher than the free-electron value of 2/3. As the temperature drops below 200 K, $\Omega_e$ gradually rises, plateaus below 100 K, and rises sharply below 40 K. The rise in $\Omega_e$ below 40 K is consistent with a Kondo-derived enhancement of the carrier mass that is evident in specific-heat and thermal-expansion data. The data in the temperature range 8 to 40 K vary with $T$ as $\Omega_e = a/(T+T_\Omega)$, with $T_\Omega = 6.0 \pm 0.5$ K and $a = 290 \pm 7$. The scaling temperature $T_\Omega$ is similar to the Kondo temperature estimated from the Sommerfeld coefficient at $T_N$. The peak at $\sim 8.5$ K and the subsequent drop at lower temperatures are presumably connected with the influence of magnetic order. Assuming that without magnetic ordering the scaling function for $\Omega_e$ from the range 8 to 40 K would be valid down to 0 K an extrapolation of $\Omega_e$ produces a $T=0$ electronic Grüneisen parameter of $\Omega_{hf} \equiv \Omega_e(T \to 0) = a/T_\Omega = 48 \pm 6$, quite close to our simple estimation of $\Omega_e$ ($\sim 42$) for a heavy-fermion system with $T_K = 10$ K. This value is more than an order of magnitude greater than that of a normal metal.[44] Thus, while $\gamma$ is enhanced by a factor of more than 100 relative to that of a normal metal, the electronic component of the thermal expansion coefficient is enhanced by another order of magnitude. $Ce_2RhIn_8$'s extrapolated $T=0$ electronic Grüneisen parameter is of the same order of magnitude as that of the heavy-electron compounds $CeBe_{13}$ ($\Omega_{hf} \sim 17$),[37] $UAl_2$ ($\Omega_{hf} \sim 20$),[38] $URu_2Si_2$ ($\Omega_{hf} \sim 25$),[45] and $CeCu_2Si_2$ ($\Omega_{hf} \sim 54$),[46] but is small compared to that of $CeAl_3$ ($\Omega_{hf} \sim -200$)[47] and $CeRu_2Si_2$ ($\Omega_{hf} \sim 190$).[25]

The estimated $\Omega_{hf}$ value can be used to calculate the pressure dependence of the Sommerfeld coefficient, $d\gamma/dp$. Using once again the bulk modulus for $CeRhIn_5$[42] we can predict as a first approximation that the linear term in the specific-heat decreases with pressure at the rate equal to $d\gamma/dT = -(1/B_T)\Omega_{hf}\gamma = -25$ mJ/mole-Ce K$^2$/kbar, i.e., $\simeq -6\%$ of $\gamma$ per kbar. This value is quite similar to the rate for $CeCu_6$ ($\sim -8\%$)[48,49] and much smaller than for $CeRu_2Si_2$, where the large $\Omega_{hf} = 190$ implies a large $d\gamma/dT = -19\%$ of $\gamma$ per kbar.[25]

Given the CEF level scheme outlined in the preceding section, crystalline-electric-field excitations should dictate the magnetic and temperature dependences of $\Omega_e$ above roughly 40 K. When a single excitation dominates the thermodynamics of a system within a given temperature range the measured electronic Grüneisen parameter will be a reflection of that dominant mechanism. The plateau between 40 and 90 K in $\Omega_e$ and the gradual drop in $\Omega_e$ above 100 K must then reflect CEF effects. As such, the Grüneisen parameter associated with CEF excitations appears to achieve a maximum value of $\Omega_{CEF} \approx 6$ below 80 K. The pressure dependence of the CEF energy splitting parameter $\Delta_1$ can be determined from $d\Delta_1/dp = \Delta_1 \Omega_{CEF}/B_T$. The estimated rate is small ($d\Delta_1/dp \approx 0.6$ K/kbar), corresponding to a relative sensitivity of only 0.8% per kbar of pressure. Although the scatter in the $\Omega_e$ data above 100 K precludes a determination of $d\Delta_2/dp$ it is clear that this quantity will also be positive. Within the framework of a point-charge model $\Delta$ is inversely proportional to the interatomic distance, so these positive values for $d\Delta/dp$ are not surprising. In some heavy-fermion systems electron screening can lead to a pressure-induced decrease in $\Delta$,[50] as is the case for $CeRu_2Si_2$.[25]

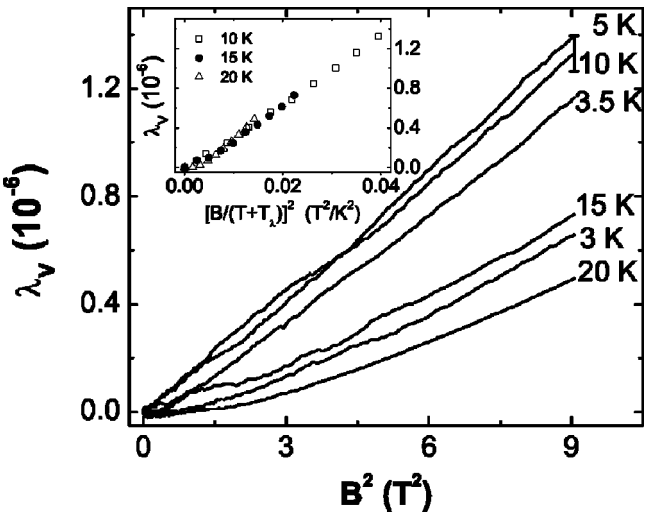


FIG. 8. Paramagnetic volume magnetostriction field sweeps plotted as a function of $B^2$ for $T = 3$, 3.5, 5, 10, 15, and 20 K. The data at 10, 15, and 20 K are plotted in the inset as a function of the scaling parameter $[B/(T+T_\lambda)]^2$, where $T_\lambda = 5 \pm 1$ K. The error bar shows estimated error connected with the value of $\lambda_V(B = 3\ \mathrm{T})$ at 10 K.

### E. Magnetostriction and competing energy scales

A careful analysis of the anomalously large magnetostriction exhibited by $Ce_2RhIn_8$ in the paramagnetic regime can provide important insights into the thermodynamic nature of the competing interactions that are present in this compound. The 10 K volume magnetostriction data shown in Fig. 3(b) vary quadratically with the applied field, are positive, and correspond to a one-part in $10^6$ change in the sample volume in 3 T. This large sample volume change in the presence of an applied field is tied to the close connection between the Kondo interaction and unit-cell volume. An expression that relates a paramagnet's volume magnetostriction to key physical quantities can be obtained by combining the Maxwell relation $\partial V/\partial H = -\partial M/\partial p$ with the definition of the bulk modulus, $B_T = -V\partial p/\partial V$. For a paramagnet ($\chi = M/H$) the volume magnetostriction varies with $H$ as $\lambda_V = S_V H^2$, where the magnetostriction coefficient $S_V$ is given by

$$S_V = \frac{1}{2B_T}\frac{\partial \chi}{\partial V}. \tag{13}$$

A simple calculation of the estimated magnetostriction for copper yields a coefficient $S_V = 4 \times 10^{-11}$ T$^{-2}$; this magnetostriction corresponds to a length change for a 1-mm-long sample in 10 T of only 0.01 Å, a quantity that is too small to measure even with a carefully designed capacitive dilatometer. In comparison, the 10 K $Ce_2RhIn_8$ magnetostriction data in Fig. 3(b) correspond to a volume magnetostriction coefficient $S_V = 1.4 \times 10^{-7}$ T$^{-2}$, a value that is roughly four orders of magnitude greater than the estimate for Cu. The experimentally observed length change at 3 T in the 1-mm-thick $Ce_2RhIn_8$ crystal was $\Delta l \approx 10$ Å; this length change is easily detected with a capacitive dilatometer.

As indicated above, the magnetostriction of a paramagnet is expected to vary quadratically with the applied field. To show that this is the case, the volume magnetostriction of $Ce_2RhIn_8$ in the paramagnetic regime is plotted as a function of $B^2$ in Fig. 8. As expected, the data vary linearly with $B^2$ from just above $T_N$ to 20 K, the highest temperature where magnetostriction data were collected. Some deviation from $\lambda_V \propto B^2$ scaling is evident as the system approaches the AFM ordering transition. This scaling breakdown most likely reflects the influence of magnetic fluctuations close to the ordering transition. Deviation from the quadratic scaling behavior is also evident at 15 and 20 K, although the overall trend is that magnetostriction isotherms are nearly parabolic in *B*. The volume magnetostriction in the higher-temperature part of paramagnetic region follows the simple scaling relationship:

$$\lambda_V = A\left(\frac{H}{T+T_\lambda}\right)^2, \tag{14}$$

which was previously found to describe the magnetostriction of rare-earth metals with unstable $4f$ shells.[21] $A$ and $T_\lambda$ are fitting constants, and $T_\lambda$ is often roughly equal to the Kondo temperature.[21] For $Ce_2RhIn_8$ the volume magnetostriction measured at $T = 10$ K, 15 K, and 20 K collapses onto a straight line (see inset to Fig. 8) with $T_\lambda = 5 \pm 1$ K. Low-temperature measurements of the specific-heat give the Sommerfeld coefficient, $\gamma \simeq 400$ mJ/mole-Ce K$^2$, corresponding to a single impurity Kondo temperature $T_K \approx 10$ K.[10] Hence $T_\lambda$ and $T_K$ are quite similar. Below 5 K the scaling behavior [Eq. (14)] is broken in the sense that $\lambda$ is still proportional to $B^2$ but it no longer increases with decreasing temperature. This is undoubtedly due to magnetic fluctuations present above $T_N$ that also give rise to a maximum in $\chi$ near $T_{max} = 5$ K. The similar maximum in $\chi(T)$ found in $CeRhIn_5$ at 7.5 K was explained[20] in terms of the susceptibility of a square two-dimensional $S = 1/2$ spin Heisenberg system which is known to exhibit a maximum in $\chi(T)$ at $T_{max} \approx 0.93|J|$.[51] For $Ce_2RhIn_8$, $T_N = 2.8$ K leads to the value $|J| \approx 2T_N/[S(S+1)] \approx 7.5$ K and hence $T_{max} \approx 7$ K. This is close to the value actually observed, so it is possible that a similar explanation is also valid for more three-dimensional $Ce_2RhIn_8$.

The underlying significance of the temperature scaling exhibited by the magnetostriction data between 10 and 20 K can be determined by examining the link between the electronic Grüneisen parameter, the magnetostriction, and the magnetic susceptibility. If we assume that the magnetic and thermal degrees of freedom in $Ce_2RhIn_8$ are independent, the most general assumption about the nature of the system's electronic free energy $F_e$ is to express it as $F_e = -Nk_BTf(T/T_0, H/H_0)$, where $T_0$ and $H_0$ are thermal and magnetic scaling parameters.[52] The low-field quadratic magnetostriction coefficient for such a free-energy functional is[53]

$$S_V = \frac{1}{2B_TV}\left[\chi(2\Omega_H - \Omega_e) + T\frac{\partial\chi}{\partial T}\Omega_e\right], \tag{15}$$

where the magnetic and electronic Grüneisen parameters are defined by $\Omega_H = -\partial \ln H_0/\partial \ln V$ and by $\Omega_e = -\partial \ln T_0/\partial \ln V$, respectively. $Ce_2RhIn_8$'s magnetic Grüneisen parameter can be determined experimentally via Eq. (15) by combining magnetostriction $\Omega_e$ and magnetic susceptibility data. The resulting values for $\Omega_T$ between 3 and 20 K are depicted as solid diamonds in Fig. 7; as with nearly all other heavy-fermion compounds, within experimental errors $\Omega_H = \Omega_e$ at all temperatures. This indicates that the thermal and magnetic energy scales are equivalent in $Ce_2RhIn_8$ so that the electronic free energy can be scaled with a single parameter $T_0 \approx T_K$. With a single scaling parameter, and when the last term in Eq. (15) can be ignored (i.e., when $\chi \gg T\ \partial\chi/\partial T$), the quadratic magnetostriction coefficient simplifies to

$$S_V \approx \frac{\chi\Omega_e}{2B_TV}. \tag{16}$$

This equation shows the direct connection between the large magnetostriction and electronic Grüneisen parameter exhibited by $Ce_2RhIn_8$; both quantities are large because of the underlying thermodynamics surrounding the Kondo effect.

Does Eq. (16) explain the temperature-dependent scaling evidenced by the magnetostriction data as plotted in the inset to Fig. 8 ? Between 10 and 20 K the volume magnetostriction scales with temperature as $S_V \propto (T+T_\lambda)^{-2}$, with $T_\lambda = (5 \pm 1)$ K. Over the same temperature range the electronic Grüneisen parameter varies with temperature as $\Omega_e \propto (T+T_\lambda)^{-1}$, with $T_\Omega = 6.0 \pm 0.5$ K. Within experimental uncertainty, $T_\Omega = T_\lambda$. Hence, the electronic Grüneisen parameter and volume magnetostriction both scale with a single energy parameter that is comparable to the Kondo temperature. Since Eq. (16) indicates that $S_V \propto \chi\Omega_e$, it follows that the magnetic susceptibility should scale with temperature as $\chi \propto (T-T_\chi)^{-1}$, with $T_\chi \approx -T_\Omega$. The low-temperature magnetic susceptibility of many heavy-fermion compounds follows this functional form, with the scaling parameter $|T_\chi|$ comparable to the Kondo temperature inferred from the low-temperature electronic contribution to the specific heat.[50] In the case of $Ce_2RhIn_8$ the magnetic susceptibility is strongly anisotropic below 40 K. $\chi_{ab}$ exhibits a broad maximum centered at 4.5 K whereas $\chi_c$ is essentially temperature independent below 4.5 K. Between 8 and 60 K $\chi_{ab}(T)$ scales with temperature in the expected manner, $\chi(T) \propto (T-T_\chi)^{-1}$, but with a scaling temperature $T_\chi = -48$ K. This is an order of magnitude larger than the value expected based on the temperature scaling evident in $\lambda_V$ and $\Omega_e$ data.

Rather than indicating a breakdown in thermodynamic scaling in $Ce_2RhIn_8$, the dissimilar energy scales evident in $\lambda_V(T)$ (or $\Omega_e(T)$) and $\chi(T)$ data indicate that something other than the Kondo interaction is determining the temperature dependence of the magnetic susceptibility. Above 200 K the in-plane magnetic susceptibility of $Ce_2RhIn_8$ exhibits Curie-Weiss behavior with a paramagnetic $\theta$ of $-65$ K, indicating that antiferromagnetic exchange dominates the susceptibility. The low-temperature scaling parameter $T_\chi$ is nearly the same as the high-temperature paramagnetic $\theta$, suggesting that $T_\chi$ reflects a combination of RKKY-driven magnetic exchange possibly coupled with CEF interactions. The discrepancy between the thermal scaling energies in $\chi$, $\lambda_V$, and $\Omega_e$ can be rectified if we assume that the electronic free energy is the sum of terms that reflect separately the Kondo and exchange/CEF interactions, $F_e \propto f_1(T/T_K) + f_2(T/T_{mag})$, where $T_{mag}$ reflects the aggregate influences of antiferromagnetic exchange and CEF interactions. With this electronic free-energy ansatz the magnetostriction still varies quadratically with field. In the low-field limit the quadratic magnetostriction coefficient is the sum of contributions from Kondo and magnetic exchange interactions, $S_V \propto \chi_K \Omega_K + \chi_{mag}\Omega_{mag}$. In this expression $\chi_K$ and $\Omega_K$ are the magnetic susceptibility and the electronic Grüneisen parameter stemming from Kondo interactions, while $\chi_{mag}$ and $\Omega_{mag}$ are the corresponding terms stemming from magnetic exchange and CEF interactions. The differing thermal scaling parameters evident in the measured $\lambda_V(T)$, $\Omega_e(T)$, and $\chi(T)$ data indicate that while magnetic exchange and CEF interactions dominate the susceptibility below roughly 40 K, Kondo interactions dominate the magnetostriction. For this to be true $\Omega_K$ must be significantly larger than the electronic Grüneisen parameter associated with spin fluctuations. This is borne out by the fact that observed electronic Grüneisen parameters at low temperatures in Kondo systems are always much larger than at higher temperatures where magnetic exchange and crystal-field interactions dictate thermodynamic properties.[50] This is certainly consistent with the sharp rise evident in the measured electronic Grüneisen parameter of $Ce_2RhIn_8$ below 40 K.

## V. CONCLUSIONS

The complex thermodynamic properties of $Ce_2RhIn_8$ reflect the underlying interplay between magnetic exchange, Kondo, and symmetry-derived crystal-field interactions. RKKY interactions give rise to antiferromagnetic order below 2.8 K with a reduced ordered moment and a complicated $H$-$T$ phase diagram. In the paramagnetic phase just above $T_N$ Kondo interactions produce a renormalized carrier-mass state that strongly influences the specific-heat, magnetostriction, and thermal expansion. The electronic Grüneisen parameter becomes quite large in this temperature regime, and the temperature dependence of both $\Omega_e$ and the volume magnetostriction exhibit a characteristic energy scale that is comparable to the Kondo temperature as estimated from the Sommerfeld coefficient just above $T_N$. In contrast, the magnetic susceptibility in this same temperature regime appears to be controlled by magnetic exchange and CEF interactions. Above roughly 40 K single-impurity Kondo interactions become less important, only influencing the temperature dependence of the resistivity. In contrast, CEF effects dictate the thermal expansion and dominate the electronic Grüneisen parameter in this same temperature regime. These results are quite similar to the thermodynamics of the single-layer compound $CeRhIn_5$. Both compounds share similar CEF level schemes,[29,30] AFM order with similar ordering temperatures and complex $H$-$T$ phase diagrams,[5] a heavy-electronic state that grows in importance below 20 K, and pressure-induced superconductivity that appears to be mediated by spin fluctuations.[6] While the thermodynamic analysis presented in this paper only indirectly addresses the origins of energy scaling behavior, such analysis is crucial in determining and untangling the important energy scales present in the $Ce_nRhIn_{3n+2}$ family of compounds.

## ACKNOWLEDGMENTS

We would like to thank J. Lawrence, A. Llobet, and M. Nicklas for useful discussions. This work was performed under the auspices of the U.S. Department of Energy.

*Present address: Instituto de Física ''Gleb Wathagin,'' UNICAMP, 13083-970 Campinas, Brazil.

[1] For a review see N. Grewe and F. Steglich, in *Handbook on the Physics and Chemistry of Rare Earth*, edited by K. A. Gschneider, Jr. and L. Eyring (Elsevier, Amsterdam, 1991), Vol. 14, p. 343.

[2] S. Doniach, in *Valance Instabilities and Related Narrow Band Phenomena*, edited by R. D. Parks (Plenum, New York, 1977), p. 169.

[3] M.F. Hundley, J.L. Sarrao, J.D. Thompson, R. Movshovich, M. Jaime, C. Petrovic and Z. Fisk, Phys. Rev. B **65**, 024401 (2001).

[4] J.D. Thompson, M. Nicklas, A. Bianchi, R. Movshovich, A. Llobet, W. Bao, A. Malinowski, M.F. Hundley, N.O. Moreno, P.G. Pagliuso, J.L. Sarrao, S. Nakatsujii, Z. Fisk, R. Borth, E. Lengyl, N. Oeschler, G. Sparn, and F. Steglich, Physica B **329**, 446 (2003).

[5] A.L. Cornelius, P.G. Pagliuso, M.F. Hundley, and J.L. Sarrao, Phys. Rev. B **64**, 144411 (2001).

[6] M. Nicklas, V.A. Sidorov, H.A. Borges, P.G. Pagliuso, C. Petrovic, Z. Fisk, J.L. Sarrao, J.D. Thompson, Phys. Rev. **67**, 020506(R) (2003).

[7] These values are slightly higher than given in Ref. 12.

[8] A. Malinowski, M. F. Hundley, N. O. Moreno, J. L. Sarrao, and J. D. Thompson (unpublished).

[9] A.L. Cornelius, A.J. Arko, J.L. Sarrao, M.F. Hundley, and Z. Fisk, Phys. Rev. B **62**, 14 181 (2000).

[10] V.T. Rajan, Phys. Rev. Lett. **51**, 308 (1983).

[11] G.R. Stewart, Rev. Mod. Phys. **56**, 755 (1984).

[12] W. Bao, P.G. Pagliuso, J.L. Sarrao, J.D. Thompson, Z. Fisk, and J.W. Lynn, Phys. Rev. B **64**, 020401 (2001).

[13] J.M. Lawrence and S.M. Shapiro, Phys. Rev. B **22**, 4379 (1980); A. Benoit, J.X. Boucherle, P. Convert, J. Flouquet, J. Palleau, and J. Schweizer, Solid State Commun. **34**, 293 (1980).

[14] W. Bao, P.G. Pagliuso, J.L. Sarrao, J.D. Thompson, Z. Fisk, J.W.

Lynn, and R.W. Erwin, Phys. Rev. B **62**, 14 621 (2001); **63**, 219901(E) (2001); **67**, 099903(E) (2003).
[15] P.C. Canfield and Z. Fisk, Philos. Mag. B **65**, 1117 (1992).
[16] R.T. Macaluso, J.L. Sarrao, N.O. Moreno, P.G. Pagliuso, J.D. Thompson, F.R. Fronczek, M.F. Hundley, A. Malinowski, and J.Y. Chan, Chem. Mater. **15**, 1394 (2003).
[17] F.R. Kroeger and C.A. Swenson, J. Appl. Phys. **48**, 853 (1977).
[18] LakeShore Cryotronics, Inc., 64 East Walnut Street, Westerville, Ohio 43081, USA.
[19] See, for instance, E. S. R. Gopal, *Specific Heats at Low Temperatures* (Plenum Press, New York, 1966).
[20] J.D. Thompson, R. Movshovich, Z. Fisk, F. Bouquet, N.J. Curro, R.A. Fisher, P.C. Hammel, H. Hegger, M.F. Hundley, M. Jaime, P.G. Pagliuso, C. Petrovic, N.E. Phillips, and J.L. Sarrao, J. Magn. Magn. Mater. **226–230**, 5 (2001).
[21] J. Zieglowski, H.U. Häfner, D. Wohlleben, Phys. Rev. Lett. **56**, 193 (1986).
[22] E. Moshopoulou (private communication).
[23] A. Llobet, W. Bao, N. O. Moreno, J. L. Sarrao, J. D. Thompson, and J. W. Lynn (unpublished).
[24] B. Coqblin and J.R. Schrieffer, Phys. Rev. **185**, 847 (1969).
[25] A. Lacerda, A. de Visser, P. Haen, P. Lejay, and J. Flouquet, Phys. Rev. B **40**, 8759 (1989).
[26] See, for instance, D. J. Newman, and Betty Ng, *Crystal Field Handbook* (Cambridge University Press, Cambridge, 2000), p. 9.
[27] T. Ohama, H. Yasuoka, D. Mandrus, Z. Fisk, and J.L. Smith, J. Phys. Soc. Jpn. **64**, 2628 (1995).
[28] P. Morin, J. Rouchy, and D. Schmitt, Phys. Rev. B **37**, 5401 (1988).
[29] A.D. Christianson, J.M. Lawrence, P.G. Pagliuso, N.O. Moreno, J.L. Sarrao, J.D. Thompson, P.S. Riseborough, S. Kern, E.A. Goremychkin, and A.H. Lacerda, Phys. Rev. B **66**, 193102 (2002).
[30] P.G. Pagliuso, N.J. Curro, N.O. Moreno, M.F. Hundley, J.D. Thompson, J.L. Sarrao, and Z. Fisk, Physica B **320**, 370 (2002).
[31] The best fit is obtained with $\lambda_{ab}=-35$ (emu/mole)$^{-1}$, $\lambda_c=-23$ (emu/mole)$^{-1}$, $\Delta_1=71$ K, $\Delta_2=194$ K, and $\eta=0.86$. A small isotropic constant term, $\chi_0=1.95\times10^{-4}$ emu/mole, was also used to improve the fit. This $\chi_0$ term may stem from a Pauli-paramagnetic contribution.
[32] A.P. Murani, A.D. Taylor, R. Osborn, and Z.A. Bowden, Phys. Rev. B **48**, 10 606 (1993).
[33] P.G. Pagliuso, J.D. Thompson, M.F. Hundley, and J.L. Sarrao, Phys. Rev. B **62**, 12 266 (2000).
[34] T. H. K. Barron and G. K. White, *Heat Capacity and Thermal Expansion at Low Temperatures* (Kluwer Academic/Plenum Publishers, New York, 1999), p. 17.
[35] J.D. Thompson, M.F. Hundley, and J.L. Sarrao, J. Alloys Compd. **271–273**, 335 (1998).
[36] G.K. White and J.G. Collins J. Low Temp. Phys. **7**, 43 (1972).
[37] J.P. Kappler and A. Meyer, J. Phys. F: Met. Phys. **9**, 143 (1979).
[38] M. S. Wire, Ph. D. thesis, University of California, San Diego, 1985.
[39] K. Andres, J.E. Graebner, and H.R. Ott, Phys. Rev. Lett. **35**, 1779 (1975).
[40] M. Lang, Ph. D. thesis, University Darmstadt, 1991.
[41] Constant-pressure, rather than constant-volume, specific-heat data are used here to determine $\Omega_{el}$. The error this introduces is minor because the difference between $C_p$ and $C_V$ is less than 1% below 50 K, and only $\sim 3\%$ at room temperature.
[42] R.S. Kumar, H. Kohlmann, B.E. Light, A.L. Cornelius, V. Raghavan, T.W. Darling, and J.L. Sarrao, cond-mat/0209005.
[43] The error bars shown in Fig. 7 depict the uncertainties estimated from the uncertainties connected with $\alpha$, $c_p$, and $\chi$ measurements. The value of $B_T$ influences both $\Omega_e$ and $\Omega_H$ in the same way.
[44] See, for instance, T. H. K. Barron and G. K. White, *Heat Capacity and Thermal Expansion at Low Temperature* (Ref. 34), Tables 6.1, 6.2, and 6.3.
[45] A. de Visser, F.E. Kayzel, A.A. Menovsky, J.J.M. Franse, J. van den Berg and G.J. Nieuwenhuys, Phys. Rev. B **34**, 8168 (1986).
[46] J. D. Thompson and J.M. Lawrence, *Handbook on the Physics and Chemistry of Rare Earth* (Ref. 50), Table 5, p. 429.
[47] R. Takke, M. Niksch, W. Assmus, B. Lüthi, R. Pott, R. Schefzyk, and D.K. Wohlleben, Z. Phys. B: Condens. Matter **44**, 33 (1981), and references cited therein; see also discussion in J.D. Thompson and J.M. Lawrence, *Handbook on the Physics and Chemistry of Rare Earth* (Ref. 50), p. 434.
[48] A. de Visser, A. Lacerda, P. Haen, J. Flouquet, F.E. Kayzel, and J.J.M. Franse, Phys. Rev. **39**, 11 301 (1989).
[49] R.A. Fisher, S.E. Lacy, C. Marcenat, J.A. Olsen, N.E. Philips, J. Fouquet, A. Amato, and D. Jaccard, Jpn. J. Appl. Phys. **26**, 482 (1987).
[50] J. D. Thompson and J. M. Lawrence, in *Handbook on the Physics and Chemistry of Rare Earth*, edited by K. A. Gschneider, Jr. and L. Eyring (Elsevier, Amsterdam, 1994), Vol. 19, Chap. 133, p. 383.
[51] L.J. de Jongh and A.R. Miedema, Adv. Phys. **23**, 1 (1974).
[52] P. Thalmeier and P. Fulde, Europhys. Lett. **1**, 367 (1986).
[53] J.D. Thompson and J.M. Lawrence, *Handbook on the Physics and Chemistry of Rare Earth* (Ref. 50), p. 436, and references cited therein.